Measuring the scattering parameters of tissues from quantitative phase imaging of thin slices

Huafeng Ding,[1] Zhuo Wang,[1] Xing Liang,[1] Stephen A. Boppart,[1] Krishna Tangella,[2] and Gabriel Popescu[1,*]

[1]*Department of Electrical and Computer Engineering, Beckman Institute for Advanced Science and Technology, University of Illinois at Urbana-Champaign, Urbana, Illinois 61801, USA*

[2]*Department of Pathology, Christie Clinic and University of Illinois at Urbana-Champaign, Urbana, Illinois 61801, USA*

**Corresponding author: gpopescu@illinois.edu*

Received March 23, 2011; revised May 6, 2011; accepted May 12, 2011;
posted May 13, 2011 (Doc. ID 144661); published June 13, 2011

We employed the scattering-phase theorem recently derived in our laboratory to extract tissue scattering properties from quantitative phase images. Using tissue path-length maps that contain nanoscale information about the tissue, the scattering mean free path l_s and anisotropy factor g were measured in a spatially resolved manner.

OCIS codes: 290.5820, 180.3170.

Light scattering from tissues has attracted extensive research interest, especially due to the potential it offers for *in vivo* diagnosis [1]. The starting point in light-scattering-based diagnosis is that normal and diseased tissues are characterized by scattering parameters that are measurably different. Translating such methods to the clinic require knowledge of the optical properties associated with both healthy and diseased tissues. However, the direct measurement of these scattering parameters, i.e., the scattering mean free path l_s and anisotropy factor g, is extremely challenging [2–4]. In the absence of absorption, the scattering mean free path, l_s, is the average distance between two adjacent scattering events or the distance over which the unscattered light decreases to 1/e of its original power. The anisotropy factor is the average cosine of the scattering angle, $g = \langle \cos\theta \rangle$, and is used to obtain the transport mean free path, $l_t = l_s/(1-g)$, which normalizes l_s to larger values to account for forward-biased scattering (i.e., $g > 0$).

In response to this challenge, we have recently proposed a method to extract the scattering properties of bulk tissues from quantitative phase images of slices [5]. Quantitative phase imaging (QPI), in which maps of path-length shifts across transparent samples are measured interferometrically, has become a dynamic area of study, as it provides information of both refractive index and nanoscale structure in cells and tissues (for reviews on methods and applications, see, e.g., [6,7]). Recently, there has been an effort to use QPI to attack clinical problems, such as blood screening [8–11] and tissue diagnosis [12–14]. In this Letter, for the first time to our knowledge, we spatially map the tissue slices in terms of the *scattering mean free path*, l_s, and the *anisotropy factor*, g, which are the main tissue parameter ingredients in light transport theory.

From the *scattering-phase theorem* derived in [5], the scattering mean free path l_s averaged over a certain area across a tissue slice is directly related to the variance of the phase within that region, while the anisotropy factor g is proportional to the variance of the *phase gradient* intensity. This theorem provides a mathematical relationship between l_s and g on one hand and the statistics of phase-shift distribution associated with a thin tissue slice, as measured via QPI [5],

$$l_s = \frac{L}{\langle \Delta\phi^2(\mathbf{r}) \rangle_{\mathbf{r}}}, \qquad g = 1 - \left(\frac{l_s}{L}\right)^2 \frac{\langle |\nabla[\phi(\mathbf{r})]|^2 \rangle_{\mathbf{r}}}{2k_0^2}. \tag{1}$$

In Eq. (1), L is the tissue slice thickness, $L \ll l_s$, $\langle \Delta\phi^2(\mathbf{r}) \rangle_{\mathbf{r}} = \langle [\phi(\mathbf{r}) - \langle \phi(\mathbf{r}) \rangle_{\mathbf{r}}]^2 \rangle_{\mathbf{r}}$ is the phase variance, with $\langle \rangle_{\mathbf{r}}$ denoting spatial average over a certain area, $k_0 = 2\pi/\lambda$, with λ the mean wavelength of light in tissue, and $|\nabla[\phi(\mathbf{r})]|^2 = (\partial\phi/\partial x)^2 + (\partial\phi/\partial y)^2$ the modulus squared of the phase gradient, with $\boldsymbol{r} = (x, y)$. Here the definition of g is extended to continuous distributions of refractive index: it is the average cosine of the scattering angle associated with a slice of thickness l_s. This way, the assumption that the tissue is made of discrete particles is removed.

In order to implement this approach experimentally, we used spatial light interference microscopy (SLIM), a new quantitative phase imaging method developed in our laboratory [15]. SLIM uses broadband light centered at 535 nm and provides highly sensitive QPI, with 0.03 nm path-length sensitivity temporally and 0.3 nm spatially [16]. Two adjacent 4 μm thick tissue biopsies, one unstained and one stained by hematoxylin and eosin (H&E) were imaged by SLIM and bright field, respectively. Figure 1 illustrates the ability of SLIM to render high transverse resolution, high phase sensitivity images of thin tissue slices. The phase information provided by SLIM is inherently averaged over the optical frequencies [17]. Thus, the scattering parameters obtained by this method will also be frequency averaged. Throughout the experiments presented here, we used a 10×, 0.3 NA objective. This limited numerical aperture effectively acts as a low-pass spatial frequency filter. The spatial averages performed in deriving the two equations in Eq. (1) are expected to be affected by this cutoff. Because tissues scatter strongly forward (g close to 1), we anticipate that the low NA is not a significant error source. However, in order to quantify this effect, we used

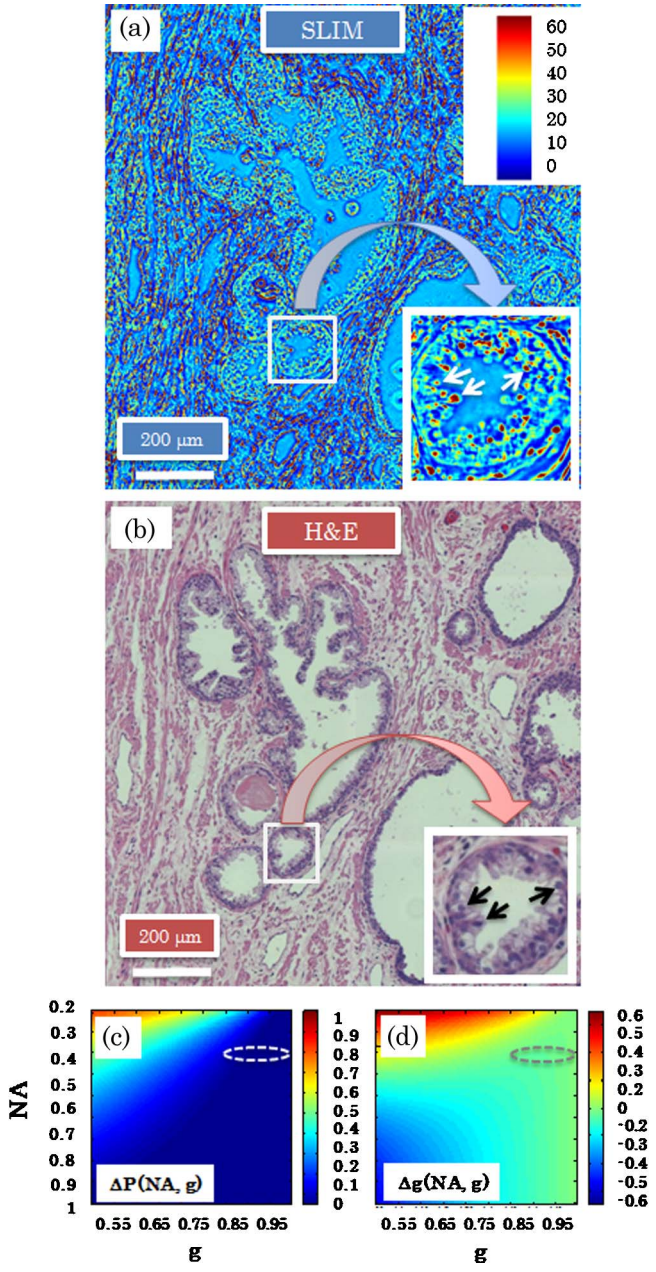

Fig. 1. (Color online) (a) Imaging of a human prostate biopsy by SLIM and (b) H&E staining. Color bar indicates path length in nanometers (to enhance details in the inset, many pixels are saturated at 60 nm). The insets show details of a normal gland, and arrows indicate epithelial cells. (c), (d) Error estimation due to limited NA: error in power versus NA and g (c); error in g versus NA and g (d).

the common Henyey–Greenstein angular distribution to calculate the respective error functions,

$$\Delta P(\mathrm{NA}, g) = 1 - \int_{\sqrt{1-\mathrm{NA}^2}}^{1} P(\cos\theta)\mathrm{d}\cos\theta, \tag{2a}$$

$$\Delta g(\mathrm{NA}, g) = 1 - \int_{\sqrt{1-\mathrm{NA}^2}}^{1} \cos\theta P(\cos\theta)\mathrm{d}\cos\theta, \tag{2b}$$

where P is the Henyey–Greenstein distribution, normalized to unit area, $P(\cos\theta) \propto (1-g^2)/(1+g^2-2g\cos\theta)^{3/2}$. In Eqs. (2a) and (2b), ΔP represents the scattered power that is not accounted for due to NA, and Δg represents the difference between the measured and true average cosine of the scattering angle (i.e., g). Figure 1 shows the two error functions. It can be seen that, in the measurement range set by our NA = 0.3 and large g values associated with tissues [ellipses in Figs. 1(c) and 1(d)], the errors are below 10% in power and 5% in g, and decrease accordingly for higher NA. We note that a systematic error in the thickness of the tissue slice will introduce errors in the l_s and g values. The tissue biopsies used in this study were sectioned using a high-precision microtome at 4 μm thickness, with <1 μm accuracy. This error of maximum 25% in the measured l_s is much higher than what our instrument can afford in terms of phase imaging. However, in all applications of medical relevance, the ratio in values for normal and diseased tissues rather than their absolute value is of interest. Measuring this ratio is thickness-independent and thus subject to much better accuracy.

We acquired QPI associated with 5 μm thick tissue slices from rat organs. The tissue was sliced frozen but thawed before imaging. The specimens were prepared according to a protocol approved by the Institutional Animal Care and Use Committee at the University of Illinois at Urbana-Champaign. Three slices from each organ of the same rat were cut in succession and imaged by SLIM. The field of view of the microscope was 0.4 mm × 0.3 mm. In order to image the cross-section of the entire organ, the specimen was translated, and a mosaic of quantitative phase images was acquired and numerically collaged together. We obtained single quantitative phase image made of hundreds of individual SLIM images. Note that this quantitative phase image covers the entire cross-section of a rat organ, with a resolution of $\sim\lambda/2\mathrm{NA} = 0.9\,\mu$m. Figure 2(a) shows one example of QPI of a tissue slice cut from a three month old rat liver.

Following Eq. (1), we calculated l_s and g in windows of 9 μm × 9 μm across the entire tissue slice. Figures 2(b) and 2(c) show the maps of l_s and g for the same rat liver in Fig. 2(a).

Our results for liver are compatible with values obtained by diffusion scattering measurements [12,18]. It is apparent that the tissue scattering parameters exhibit strong inhomogeneities across the organ, mainly due to inclusions that induce refractive index fluctuations. Note that the background l_s values are very high, indicating

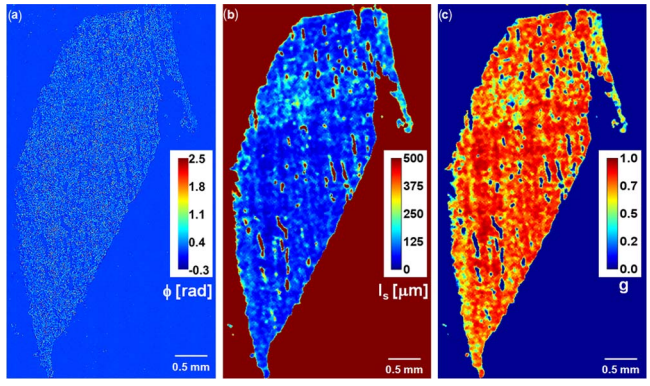

Fig. 2. (Color online) Maps of (a) ϕ, (b) l_s, and (c) g for a tissue slice across an entire rat liver; the g map is thresholded to show $g = 0$ for background. Color bars show ϕ, l_s and g, as indicated.

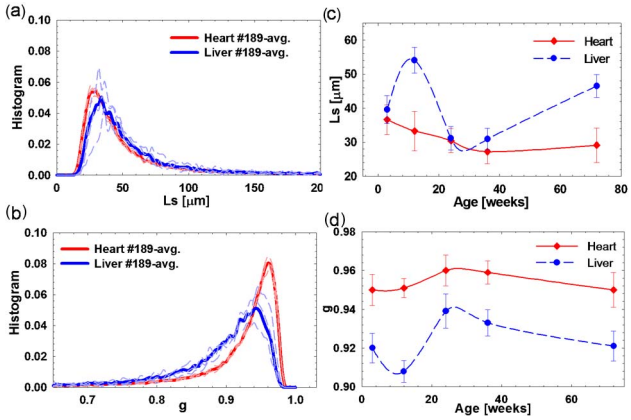

Fig. 3. (Color online) (a), (b) Histograms of l_s (a) and g (b) for rat liver and heart tissues. The faint lines indicate different measurements and thick lines show their averages. (c), (d) Evolution of the mode distributions associated with l_s (c) and g (d) for heart and liver, as indicated. Error bars show the standard deviation of measurements on three specimens.

lack of scattering, as expected. The histogram of l_s and g obtained from rat liver and heart sections are presented in Figs. 3(a) and 3(b). We found that the average l_s is smaller for heart than for liver, which indicates that the unscattered light decays faster in the heart. Furthermore, the anisotropy factor is higher for heart, which is associated with a more dominant forward scattering.

Nevertheless, our measurements uniquely underline the significant spread in the measured values for both parameters, which is an important aspect when aiming for diagnosis. We used this procedure to map rat organs at five different ages: 3 weeks, 3 months, 6 months, 9 months, and 18 months. The results are summarized in Figs. 3(c) and 3(d) in terms of the modes of the distributions. While we see variations of these modes with age, these changes are within the widths of the distributions. The only conclusions that can be drawn are probabilistic, e.g., the most probable l_s value is decreasing slightly with age in heart tissues. The most probable g values seem to remain roughly constant in time, but distinct for the both of the two organs. The apparent correlations between l_s and g, especially for liver, may suggest that both l_s and g track the morphology of the tissue with age, but it is difficult to draw a conclusion based on this limited data set.

In summary, following a recent theoretical result [5], our experimental method provides fast and spatially resolved access to tissue scattering mean free path l_s and anisotropy factor g from QPI of thin tissue slices. SLIM provides nanoscale information about the tissue structure, which in itself sets the basis for a new type of label-free diagnosis of biopsies. The knowledge of l_s and g has great impact on predicting the outcome of a broad range of scattering experiments on large samples. Our method allows building up an exhaustive database, where various tissue types, healthy and diseased, are fully characterized in terms of their scattering properties, from microscopic (organelle) to macroscopic (organ) spatial scales. With further understanding of sample preparation effects on l_s and g, such a database will be of valuable assistance when applying *in vivo* optical methods directly to patients by providing, for example, *a priori* information on relative changes expected between normal and diseased tissue parameters.

This research was supported in part by the National Science Foundation (NSF) (CAREER 08-46660) and National Cancer Institute (R21 CA147967-01). For more information, visit http://light.ece.uiuc.edu/.

References

1. A. Wax and V. Backman, eds., *Biomedical Applications of Light Scattering* (McGraw-Hill, 2010).
2. A. Amelink, H. J. C. M. Sterenborg, M. P. L. Bard, and S. A. Burgers, Opt. Lett. **29**, 1087 (2004).
3. D. J. Cuccia, F. Bevilacqua, A. J. Durkin, F. R. Ayers, and B. J. Tromberg, J. Biomed. Opt. **14**, 024012 (2009).
4. F. Bevilacqua, D. Piguet, P. Marquet, J. D. Gross, B. J. Tromberg, and C. Depeursinge, Appl. Opt. **38**, 4939 (1999).
5. Z. Wang, H. Ding, and G. Popescu, Opt. Lett. **36**, 1215 (2011).
6. G. Popescu, in *Methods in Cell Biology*, B. P. Jena, ed. (Academic, 2008) p. 87–115.
7. C. Depeursinge, in *Digital Holography and Three-Dimensional Display*, T.-C. Poon, ed. (Springer U.S., 2006), p. 98–143.
8. M. Mir, M. Ding, Z. Wang, J. Reedy, K. Tangella, and G. Popescu, J. Biomed. Opt. **15**, 027016 (2010).
9. Y. K. Park, M. Diez-Silva, G. Popescu, G. Lykotrafitis, W. Choi, M. S. Feld, and S. Suresh, Proc. Natl. Acad. Sci. USA **105**, 13730 (2008).
10. Y. K. Park, C. A. Best, K. Badizadegan, R. R. Dasari, M. S. Feld, T. Kuriabova, M. L. Henle, A. J. Levine, and G. Popescu, Proc. Natl. Acad. Sci. USA **107**, 6731 (2010).
11. M. Mir, Z. Wang, K. Tangella, and G. Popescu, Opt. Express **17**, 2579 (2009).
12. H. Ding, F. Nguyen, S. A. Boppart, and G. Popescu, Opt. Lett. **34**, 1372 (2009).
13. Z. Wang, K. Tangella, A. Balla, and G. Popescu, "Tissue refractive index as marker of disease," Proc. Natl. Acad. Sci. USA, submitted for publication.
14. H. F. Ding, Z. Wang, F. Nguyen, S. A. Boppart, and G. Popescu, Phys. Rev. Lett. **101**, 238102 (2008).
15. Z. Wang, L. J. Millet, M. Mir, H. Ding, S. Unarunotai, J. A. Rogers, M. U. Gillette, and G. Popescu, Opt. Express **19**, 1016 (2011).
16. Z. Wang, I. S. Chun, X. L. Li, Z. Y. Ong, E. Pop, L. Millet, M. Gillette, and G. Popescu, Opt. Lett. **35**, 208 (2010).
17. Z. Wang and G. Popescu, Appl. Phys. Lett. **96**, 051117 (2010).
18. V. V. Tuchin, *Tissue Optics: Light Scattering Methods and Instruments for Medical Diagnosis* (SPIE, 2007).